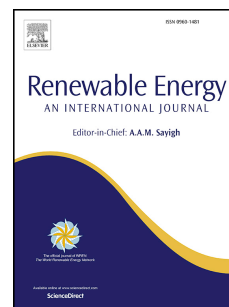


Accepted Manuscript

Effects of porous material and nanoparticles on the thermal performance of a flat plate solar collector: An experimental study

H. Javaniyan Jouybari, S. Saedodin, A. Zamzamian, M. Eshagh Nimvari, S. Wongwises



PII: S0960-1481(17)30620-1

DOI: [10.1016/j.renene.2017.07.008](https://doi.org/10.1016/j.renene.2017.07.008)

Reference: RENE 8983

To appear in: *Renewable Energy*

Received Date: 6 May 2017

Revised Date: 28 June 2017

Accepted Date: 3 July 2017

Please cite this article as: Jouybari HJ, Saedodin S, Zamzamian A, Nimvari ME, Wongwises S, Effects of porous material and nanoparticles on the thermal performance of a flat plate solar collector: An experimental study, *Renewable Energy* (2017), doi: 10.1016/j.renene.2017.07.008.

This is a PDF file of an unedited manuscript that has been accepted for publication. As a service to our customers we are providing this early version of the manuscript. The manuscript will undergo copyediting, typesetting, and review of the resulting proof before it is published in its final form. Please note that during the production process errors may be discovered which could affect the content, and all legal disclaimers that apply to the journal pertain.

Effects of porous material and nanoparticles on the thermal performance of a flat plate solar collector: An experimental study

H. Javaniyan Jouybari¹, S. Saedodin^{1*}, A. Zamzamian^{2*}, M. Eshagh Nimvari³, S. Wongwises^{4,5}

¹ Department of Mechanical Engineering, Semnan University, Semnan, Iran

² Solar Energy Group, Energy Department, Materials and Energy Research Center (MERC), Karaj, Iran

³ Faculty of Engineering, Amol University of Special Modern Technologies, Amol, Iran

⁴ Fluid Mechanics, Thermal Engineering and Multiphase Flow Research Lab. (FUTURE), Department of Mechanical Engineering, Faculty of Engineering, King Mongkut's University of Technology Thonburi, Bangmod, Bangkok 10140, Thailand

⁵ The Academy of Science, The Royal Institute of Thailand, Sanam Suea Pa, Dusit,

Bangkok 10300, Thailand

Abstract:

The thermal performance of a nanofluid flow through a flat plate solar collector with the metal porous foam filled channel is experimentally investigated. For this purpose, the SiO₂/deionized water nanofluids are prepared with volume fractions of 0.2%, 0.4% and 0.6% then their thermal behavior is examined on the porous channel collector based on the ASHRAE standard. Based on the experimental results, the thermal efficiency is improved up to 8.1% in the nanofluid flow. Using the porous media and nanofluid causes an undesirable increase in the pressure drop. To take both the heat transfer enhancement and pressure drop into consideration, a Performance Evaluation Criterion (PEC) has been used for nanofluid and porous media, separately. It is observed that as the nanoparticle volume fraction increases from 0.2% to 0.6%, the performance of nanofluid flow, PEC_{nf} , is enhanced from 1.07 to 1.34 in the lowest flow rate (0.5 lit/min). Also, the performance evaluation of the porous media, PEC_p , shows that the solar collector

* Corresponding authors.

E-mail address: S_sadodin@semnan.ac.ir, azamzamian@merc.ac.ir, Tel./fax: +98 23 33325630

performance is improved up to 0.92 with increasing the nanofluid concentration and reduction of the flow rate. Finally, the effects of SiO_2 nanoparticle size, i.e. 7 nm, 20-30 nm and 60-70 nm, have been investigated on the collector thermal performance. Results show that the efficiency curve slope parameter decreases with diminishing the nanoparticle size.

Keywords: Flat plate solar collector, Metal foam, SiO_2 nanofluid, Thermal performance, ASHRAE standard.

1. Introduction

Reduction of fossil fuel energy sources, their destructive effects on the environment and also their ascending cost have caused a great demand to sustainable energies, especially the solar energy [1,2]. Solar energy can be used in multiple of applications. One of the areas of major interest is the conversion of solar radiation to thermal energy. The solar heat can be subsequently used for different purposes includes space heating, domestic hot water, cooling or even process heating [3,4]. Solar collectors especially flat plate types are the most productive solar heaters. Flat plate solar collectors (FPSC) have comparatively great heat loss that causes lower thermal performance [5]. Using of nanoparticles such as TiO_2 , CuO , Al_2O_3 , CNTs with exceptional thermal properties is one of the key effective methods for thermal enhancement of FPSC. Nanoparticles can improve the collector thermal performance due to their significant effect on the base fluid thermal conductivity [6], and also their possible effect on the thermal boundary layer [7]. There has been great attempt to study the thermal performance of FPSC using nanofluids. More recently, an ASHRAE standard [8], has been applied by Yousefi et al. [9] for experimental analysis of a FPSC using Al_2O_3 /water nanofluid. The results showed that nanoparticle and surfactant cause an enhancement in thermal performance. Jamal-Abad et al.

[10] have studied the effect of Cu/water nanofluid on the thermal efficiency of a FPSC. Results revealed that 24% enhancement of the efficiency could be obtained with 0.05%wt of nanoparticles. Zamzamian et al. [11] have investigated the effect of Cu-synthesized/EG nanofluid on the thermal performance of a FPSC. According to their results, the efficiency of the collector was increased with growing the nanoparticle weight fraction. Effect of SiO₂/EG-water nanofluid on the thermal performance characteristics of a FPSC has been investigated by Salavati et al. [12]. Their results have elucidated the great ability of silica nanoparticle to enhance the thermal performance of FPSC, despite its low thermal conductivity. Vincely and Natarajan [13] have investigated the effect of graphene oxide/ deionized water nanofluid on the heat transfer coefficient, friction factor and collector efficiency under laminar condition. It was found that the efficiency was enhanced with the flow rate and nanoparticles mass fraction. Increasing the contact surface in flow channel is another strategy for enhancing the thermal performance in solar systems [14,15]. Cellular structures or porous mediums especially in metallic form with a great thermal conductivity rather than the working fluid and high ratio of contact surface to their volume act as a passive thermal developer. However, only a few investigations were voted to the effect of porous media on the thermal performance of FPSC. The effect of inserted porous medium substrate at the boundary side of a tubeless FPSC channel has been investigated by Al-Nimr and Alkam [16]. They found that the inserted porous substrate improved the heat transfer coefficient, especially at great overall heat losses. This enhancement could raise the thermal efficiency about 3-32%. They also mentioned that there is an optimum thickness of porous substrate which the collector has the maximum thermal performance with a moderate increase in pressure losses. In another study, Alkam and Al-Nimr [17] have numerically investigated the effect of inserted porous medium substrate at the boundary wall of a

conventional collector tube. They indicated that the porous substrate could improve the Nusselt number near to 27 times. They also found that there is an optimum thickness of porous substrate which the thermal performance is maximum with a moderate rise in pumping cost. A numerical study on the thermal effects of partial metal foam blocks in a parallel plate channel collector has been presented by Chen and Huang [18]. They used the coupled of Brinkman-Forchheimer flow model and energy equation model based on Local Thermal Non-Equilibrium (LTNE), which were solved using a stream function-vorticity analysis. Their results showed that the metal foam blocks significantly augmented the heat transfer due to the recirculation process. They also proposed a correlation to calculate the overall mean Nusselt number. In another numerical analysis, Huang et al. [19] have investigated the forced convection in pulsating flow and partial blocks of metal foams in a parallel plate channel solar collector. They solved the coupled equations through a control volume approach by utilizing a stream function-vorticity method. They showed that in a constant Reynolds number, the Local Thermal Equilibrium (LTE) condition becomes more dominant when the interfacial heat transfer between the solid-fluid phases increases. The results illustrated that the flow pulsation and partial metal foams could significantly enhance the heat transfer. The reduction of heat losses due to the natural convection in a solar collector has been experimentally investigated by Hirasawa et al. [20] with inserting a high porosity foam over the collector plate. According to their results, the heat loss reduced up to 7% by placing porous media over the collector plate. The collector inclined angle also had a small effect on the Nusselt number. Xu et al. [21] have used different analytical methods to investigate the effect of some main parameters on the heat transfer and flow in a porous channel collector. They compared Darcy, Brinkman and Frochheimer models for flow equation and also LTE and LTNE models for energy equation. Their results exhibited that by increasing the

porosity, the LTNE effect becomes weaker. They enhanced a fin analysis approach and suggested a Fin-LTE model to estimate the collector thermal performance. Rashidi et al. [22] have numerically investigated the effect of porous media on the heat transfer rate and pressure drop of a solar heat exchanger. They selected the Reynolds number, Darcy number and porous layer thickness as effective factors and analyzed them by applying Response Surface Methodology (RSM). Their results showed that the Nusselt number and pressure drop are more sensitive to the Darcy number in greater values of the porous layer thickness. Dehghan et al. [23] have been presented a semi-analytical solution for solving the heat transfer equation in a solar heat exchanger with porous media channel. They analyzed influences of the porous media shape parameter and radiation parameter on the thermal performance. Bovand et al. [24] have numerically studied the effect of porous media on the thermal enhancement and pressure drop of a solar heater. They applied volume averaged equations in the porous substrate and found that the inserted porous substrate could improve the Nusselt number. In another numerical study, Rashidi et al. [25] have investigated the sensitivity of the entropy generation in a porous media solar heat exchanger to different factors such as Darcy number, porous layer thickness, and radiation parameter. According to the results, the sensitivity of the entropy generation to the porous layer thickness was greater than the other mentioned parameters. The effect of porous medium on the performance of a double pass hybrid photovoltaic/thermal air collector was examined by Ahmed and Mohammed [26]. They concluded that using porous material could improve the outlet air temperature and thermal efficiency. Also, they reported that the compound efficiency was improved up to 3% using the porous medium.

From the literature described above, it can be noted that experimental study on the thermal performance of porous media channel FPSC with SiO_2 /deionized water nanofluid as a working

fluid has remained unstudied. As known, SiO_2 nanoparticle against its high suspension stability has a lower thermal conductivity among usual nanoparticles in thermal applications. So finding the effect of this low thermal conductivity nanoparticle on the thermal performance of a collector, which its channel filled with metal porous foam, is a great motivation of this research. The effects of different parameters including flow rate, nanoparticles concentration and size have been investigated in this study.

2. Experimental procedure

2.1. Preparation of SiO_2 / deionized water nanofluid

The SiO_2 nanoparticles with diameter of 20-30 nm have been purchased from Nanosany Corporation (Iranian Nanomaterials Pioneers Co., Mashhad, Iran) and their sizes were confirmed by Transmission Electron Microscope (i. e. TEM), as shown in Fig. 1a. The textural analyze of nanoparticles was performed with a nitrogen adsorption analyzer (BELSORP mini-II, Japan), which shown in Fig. 1b. The textural and thermophysical properties of SiO_2 nanoparticles are summarized in Table 1. SiO_2 /deionized water as the testing sample was produced using two-step procedure, without adding any surfactant. For this purpose, the desired amount of nanoparticle gradually has been added to the base fluid, and the suspension has been mixed simultaneously using magnetic stirrer for two h. Next, the partially mixed nanoparticles are dispersed ultrasonically (with Hielscher UP400S ultrasonic model, 400 W, 24 kHz) in a bath of cold water and alternative sonication time to prevent overheating of the base fluid. The ultrasonic process was applied to reduce the possibility of the agglomeration and sedimentation of nanoparticles. The visual appearance of prepared nanofluid with a solid concentration of 0.6% vol after about two months is presented in Fig. 2. No sedimentation was observed by naked eyes.

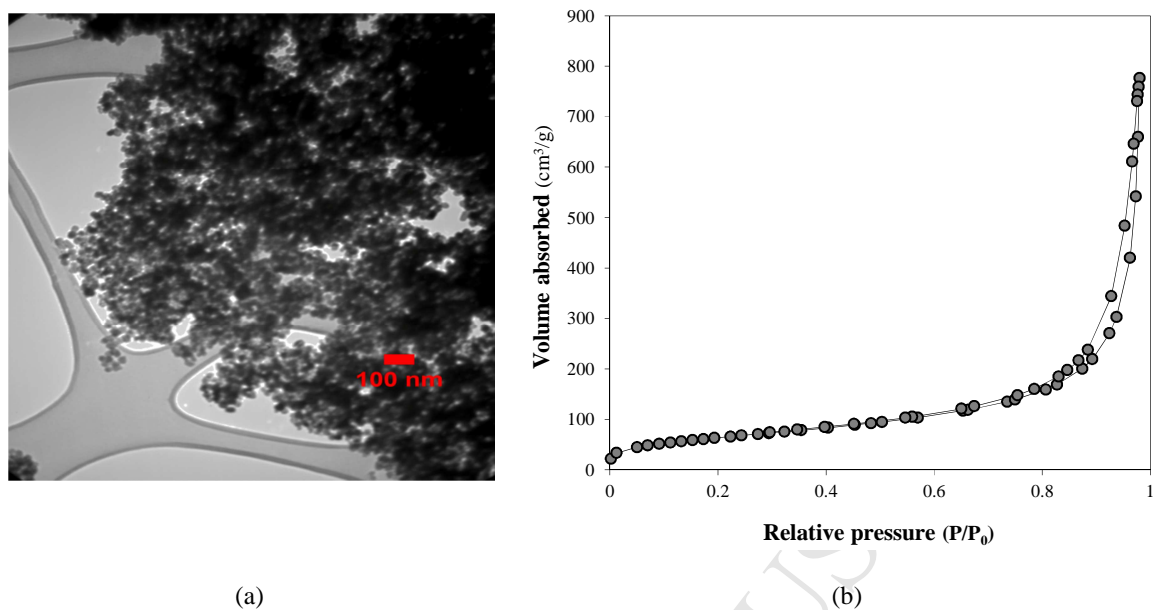


Fig. 1. (a) TEM micrograph of SiO₂ nanoparticles (Nanosany Co.), (b) N₂ adsorption/desorption isotherm of SiO₂ nanoparticles



Fig. 2. The prepared nanofluid with 0.6% vol. after two months

136

Table 1. Thermophysical and textural properties of SiO₂ nanoparticle

Nanoparticle	Thermal conductivity (W/m.k) [12]	Density (kg/m ³) [27]	Specific heat capacity (J/kg.k) [27]	BET surface area (m ² g ⁻¹)	Pore volume (cm ³ g ⁻¹)	Pore size (nm)
SiO ₂ (20-30 nm)	1.4	2200	703	232	1.2005	20.68

2.2. Thermophysical properties of nanofluid

In the present study, a thermal equilibrium between two phases of nanofluid mixture has been considered. Hence, the specific heat can be obtained based on the physical principle of the mixture rule [28,29].

$$(C_p)_{nf} = \frac{(\rho C_p)_f (1-\phi) + (\rho C_p)_{np} \phi}{\rho_{nf}} \quad (1)$$

where

$$\rho_{nf} = (1-\phi)\rho_f + \phi\rho_{np} \quad (2)$$

which ρ is density and ϕ is nanoparticles volume fraction. Thermal conductivity is calculated based on a modified model of the component mixture and is given by:

$$\frac{K_{nf}}{K_f} = \frac{K_{np} + 2K_f - 2\phi(K_f - K_{np})}{K_{np} + 2K_f + \phi(K_f - K_{np})} + \frac{\rho_{np}\phi C_p}{2K_f} \sqrt{\frac{2k_B T}{3\pi d_{np}\mu_f}} \quad (3)$$

where K is the thermal conductivity, μ is the viscosity, T is temperature, d_{np} is nanoparticle size, and k_B is Boltzmann constant. Due to considering the Brownian motion and nanoparticles aggregation, this model has a good agreement with experimental data [30].

For predicting the nanofluid viscosity, the Brinkman model is proposed [2,31]:

$$\frac{\mu_{nf}}{\mu_f} = \frac{1}{(1-\phi)^{2.5}} \quad (4)$$

2.3. Testing setup

The experimental setup of the present study consists of a flow loop, a test section, and measuring equipment. A Grundfos-UPS series pump is mounted in the flow direction to circulate the working fluid from the supply tank to collector and through the porous media. A heat exchanger

has a duty to control the inlet temperature of the working fluid to the collector. Two PT100 sensors with the precision of 0.1°C are utilized to sense the working fluid temperature in the solar collector inlet and outlet sections. Also, the absorber plate temperature is appraised with two K-type thermocouples. The flow rate is determined by a flow meter with the uncertainty of $\pm 2\%$. A TES-1333R solar power meter is used to measure the solar radiation flux. Two pressure transmitters are used at the inlet and outlet of the solar collector to measure the working fluid pressure drop with an uncertainty lower than 0.11%. Finally, a schematic of the prepared setup with its equipment is shown in Fig. 3.

The test section is a fully wetted absorber FPSC with rectangular flow channel filled with copper metal foam, according to Fig. 4. It is worthy to note that the fully filled geometry has been selected based on a numerical optimization performed in different thicknesses of metal porous media. The numerical solution is conducted for a steady, laminar and two-dimensional water flow in the composite collector channel. The flow field in the porous media and clear flow regions has been modeled by Brinkman-Forchheimer extended Darcy and Navier-Stokes equations, respectively. For energy equation, a local Thermal equilibrium has been considered between the solid matrix and fluid phases. The discretized governing equations have been solved using the finite volume method and SIMPLE algorithm. According to the numerical results, the fully filled channel has greater heat transfer to pumping power ratio and has been picked out for manufacturing as an optimum case. A photograph of the applied samples of copper foam is shown in Fig. 5. The ratio of the pore space to the total space (i. e. open porosity) of the metal porous media is 0.93. The other key quantities of metal foam and the flat plate collector are presented in tables 2 and 3, respectively.

178

Table 2. Main properties of the metal foam

Porosity	Pore Per Inch (PPI)	Length (cm)	Width (cm)	Height(cm)
0.93	20	80	7	1.3

179

Table 3. The flat plate collector technical specification

Parameter	Dimension	Unit
Collector occupied volume	$90 \times 20 \times 7 \times 10^{-6}$	m^3
Absorber length	0.8	m
Flow channel cross section	$7 \times 1.3 \times 10^{-4}$	m^2
Header pipe diameter	0.02	m
Glass thickness	0.4×10^{-2}	m
Back insulation thickness	0.026	m
Number of risers	1	
Emissivity of glass cover	0.88	
Emissivity of absorber plate	0.92	
Title angle, deg	45	
Frame	Aluminum alloy	

180

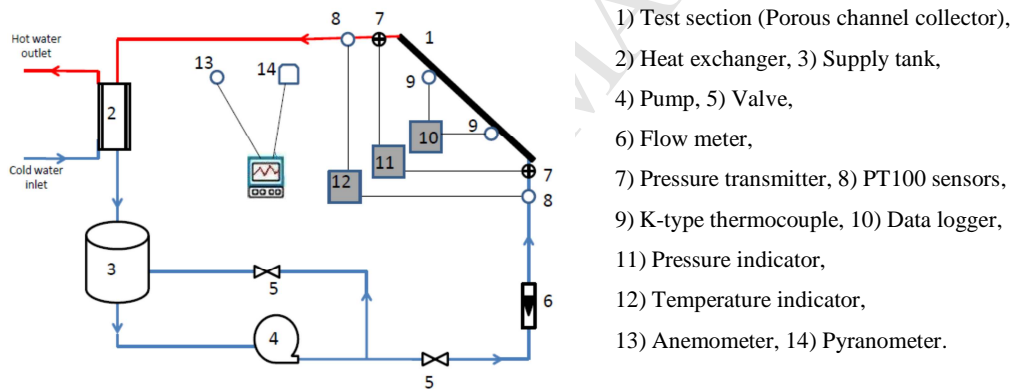


Fig. 3. A schematic diagram of the experimental set up

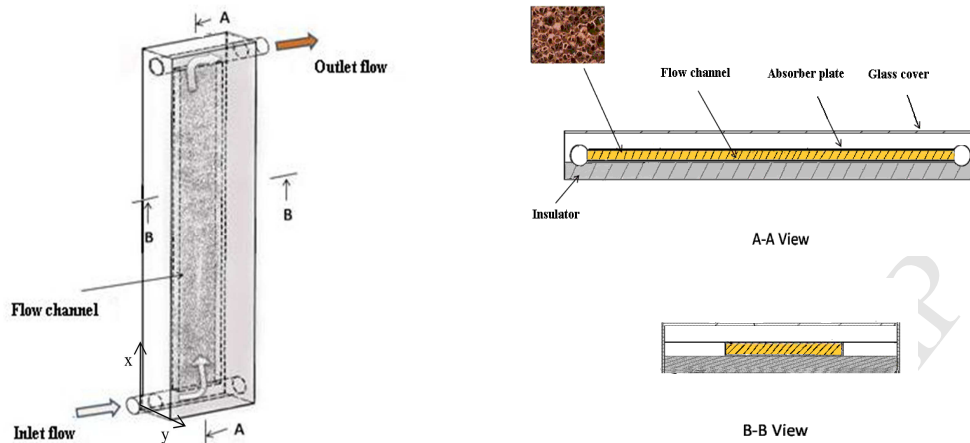


Fig. 4. The porous channel flat plate solar collector

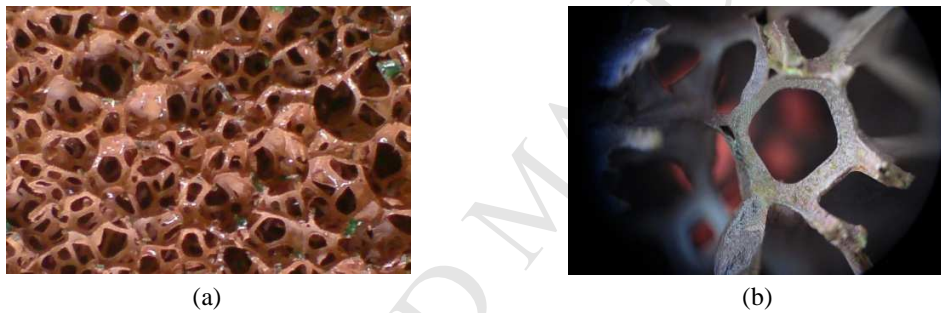


Fig. 5. Samples of open cell copper foam, (a) Cellular arrangement, (b) A single cell with regular structure.

2.4. Testing methodology

To determine the thermal performance of the porous channel collector the ASHRAE 93:2003 [8] has been used. This standard is one of the most illustrious which is often used to determine the performance of solar collectors. Some utilizations of this standard can be found in zamzamian et al. [11] for evaluating the efficiency of a FPSC and more recently, in Tajik et al. [32] for testing a parabolic trough collector. To determine the thermal efficiency based on ASHRAE, it is required to keep the steady-state condition during the testing period and in a limited time prior to

it, which called the pre-data period. According to ASHRAE, the pre-data period is 15 min and the time interval of data measurement is considered 5 min in the study. The data taken is also performed symmetric to the solar noon which decreases the number of test days. Maximum deviation in solar radiation is lower than 64 W/m^2 in each 10 min of the data measuring period. The maximum deviations of the inlet fluid temperature and ambient temperature are 1 K and $\pm 1.5 \text{ K}$, respectively, in each test period [33]. It is important to note that the climate variation in the tests run days can violate the ASHRAE standard requirements and affect the data measurement. To ensure the repeatability of experiments and achieve acceptable accuracy, each test was repeated three times.

2.4.1. Thermal performance calculation

By measuring the working fluid inlet and outlet temperatures, the net rate of useful heat gain of the working fluid can be calculated by:

$$\dot{Q}_u = \dot{m} C_p (T_{f,o} - T_{f,i}) \quad (5)$$

where \dot{Q}_u is the rate of useful heat gained, \dot{m} is the mass flow rate, $T_{f,i}$, and $T_{f,o}$ are the inlet and outlet working fluid temperatures of the solar collector, respectively. Similar to a conventional collector, the heat gain of the working fluid in the porous channel collector can be expressed regarding the absorbed energy parameter, $F_R(\tau\alpha)_e$, and efficiency curve slope parameter, $F_R U_L$, based on Duffie and Beckman [34]:

$$\dot{Q}_u = A_c F_R [I(\tau\alpha)_e - U_L(T_{f,i} - T_a)] \quad (6)$$

in which I represents the rate of incident solar irradiation on the collector per unit area, A_c is aperture area of the collector, U_L is heat loss coefficient of the collector, and T_a is the ambient temperature. F_R is heat removal factor which is expressed as follows [34]:

$$F_R = \frac{\dot{m}C_p}{A_c U_L} \left[1 - \exp\left(-\frac{A_c U_L F'}{\dot{m}C_p}\right) \right] \quad (7)$$

where F' is the collector efficiency factor. The thermal efficiency is defined as the ratio of useful extracted energy to the input solar energy. From Eq. (6) the following form of the thermal efficiency is extracted [34,35]:

$$\eta = \frac{\dot{Q}_u}{IA_c} = F_R (\tau\alpha)_e - F_R U_L \frac{(T_{f,i} - T_a)}{I} \quad (8)$$

The thermal efficiency can be plotted versus the corresponding values of reduced temperature or heat loss parameter, i. e. $\frac{(T_{f,i} - T_a)}{I}$, which a straight line will be achieved. The intersection of this line with vertical axis shows the absorbed energy parameter, and the line slope indicates the removed energy from the collector [35].

To calculate the Nusselt number, the heat transfer coefficient is obtained as [36,37]:

$$h = \frac{\dot{Q}_u}{A_p \Delta T_m} \quad (9)$$

where A_p is heat transfer surface area, and ΔT_m is the temperature difference between the wall and the bulk temperature of the working fluid. Due to the complex structure of the porous medium, evaluation of the bulk temperature of the working fluid is difficult. In this study, ΔT_m is calculated by measuring a mean temperature between the inlet and outlet flow in the porous channel, as follows [38]:

$$\Delta T_m = T_w - \left(\frac{T_{f,i} + T_{f,o}}{2} \right) \quad (10)$$

The average Nusselt number based on the hydraulic diameter is calculated as [36]:

$$Nu = \frac{hD_h}{K_{nf}} \quad (11)$$

where D_h is channel cross-sectional hydraulic diameter, and K_{nf} is effective thermal conductivity of the nanofluid. To make a reasonable comparison of the Nusselt number between empty and fully filled porous channel collectors, the Nusselt number of the fully filled channel collector is defined based on the working fluid effective thermal conductivity.

2.4.2. Efficiency uncertainty analysis

An uncertainty analysis is performed to estimate the accuracy of the measured experimental data. The thermal efficiency on its basic definition is obtained by direct measurement of volume flow rate, fluid density, specific heat, fluid temperature difference at the outlet and inlet of the collector, collector surface area, and incident radiation. The uncertainty of the efficiency, δ_η , as a dependent experimental data can be evaluated using the root-sum-square method [39]:

$$\delta_\eta = \left[\sum_{i=1}^n \left(\frac{\partial \eta}{\partial x_i} \delta_{x_i} \right)^2 \right]^{1/2} \quad (12)$$

where x_i is the input data and δ_{x_i} is the uncertainty of it. After some mathematical calculation and neglecting the variation of density, specific heat and collector surface area, the relative uncertainty of instantaneous efficiency is obtained as:

$$\frac{\delta \eta}{\eta} = \left[\left(\frac{\delta \dot{Q}}{\dot{Q}} \right)^2 + \left(\frac{\delta I}{I} \right)^2 + \left(\frac{\delta (T_{f,o} - T_{f,i})}{T_{f,o} - T_{f,i}} \right)^2 \right]^{1/2} \quad (13)$$

The relative uncertainty of the each independent variables of Eq. (13) is specified as:

$$\frac{\delta \dot{Q}}{\dot{Q}} \leq 2\% \quad (14a)$$

$$\frac{\delta(T_{f,o} - T_{f,i})}{T_{f,o} - T_{f,i}} \leq \left[\left(\frac{\delta T_{f,o}}{T_{f,o}} \right)^2 + \left(\frac{\delta T_{f,i}}{T_{f,i}} \right)^2 \right]^{1/2} \leq 1.14\% \quad (14b)$$

$$\frac{\delta I}{I} \leq 2.5\% \quad (14c)$$

Consequently, the maximum relative uncertainty of the efficiency will be about 3.39%.

3. Results and discussion

3.1. Stability of the nanofluids

In the present study, nanofluids can flow through open-cell porous structure because the size of nanoparticles with average diameter of 20-30 nm is significantly smaller than the average pore diameter of porous media which is 1.25 mm. However, it is must take into account that more obstacle of the solid matrix and greater contact surface between solid matrix and nanofluids might yield aggregation and sedimentation of nanoparticles in solid matrix pores. Since the aggregation of nanoparticles has a high influence on both the thermal conductivity and viscosity of suspensions, it is needed to examine this phenomenon in the porous media channel. Visual observation is not certainly enough for this purpose. Therefore, UV-Vis spectrophotometer measurement has been employed to characterize quantitatively the nanofluids stability. This technique was first proposed by Jiang et al. [40] for stability measurement of nanofluids. Here, two samples of nanofluids, one of them before testing in the collector and another after three hours of circulation in the porous channel collector, are prepared. Results show a great conformity between absorption spectrum of samples, which prove the porous media does not

266 have any considerable effect on the properties of nanofluids. An example of absorbance
 267 characteristics of the nanofluid with 0.6% vol. is shown in Fig. 6.

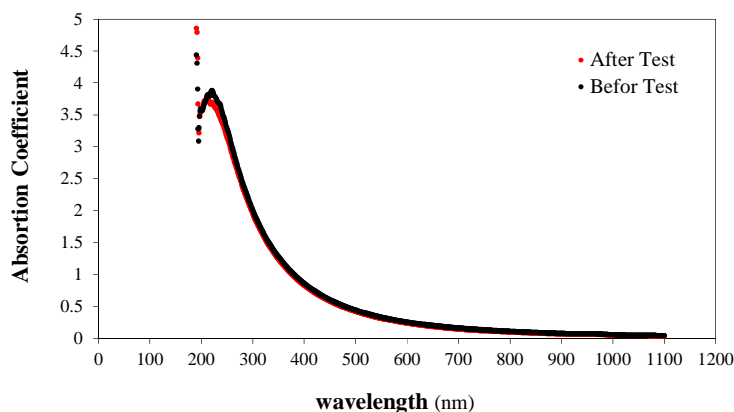


Fig. 6. UV-Vis spectrophotometer comparison of nanofluid in 0.6% vol. before and after flow through porous media channel collector

268 3.2. The effects of flow rate and nanoparticle concentration on the thermal performance

269 The effect of SiO₂ nanoparticle concentration with an average diameter size of 20-30 nm on the
 270 characteristic curves of porous channel collector is presented in Fig. 7. As shown in these curves,
 271 the nanoparticles have positive effects on the efficiency of the collector. The increase of the
 272 nanofluid concentration from 0 to 0.6% vol. leads to improve about 6% to 8% of the collector
 273 maximum efficiency (i. e. absorbed energy parameter) and consequently the related temperature
 274 increase ratio (i. e. temperature increase of the nanofluids toward the base fluid) is enhanced
 275 about 1.09 to 1.18. The thermal conductivity of silica nanoparticles is about 1.4 W/m.K [27,41],
 276 which is much smaller than other conventional nanoparticles. Despite the fact, the effect of silica
 277 nanofluid in the thermal efficiency improvement of the porous channel collector is noticeable.
 278 Hence nanofluid thermal conductivity is not the only key parameter on the heat transfer
 279 improvement. This improvement can be attributed to different mechanisms. Nanofluids have a
 280 smaller specific heat capacity rather than the base fluid, and its value decreases with increasing

the nanoparticles volume fraction. Therefore, using of nanofluids causes a higher outlet temperature. Based on the thermal efficiency definition of Eq. (8), when the increase of nanofluid outlet temperature overcomes the heat capacity reduction, can consequently lead to the thermal efficiency enhancement. Changing of the thermal boundary layer thickness is another parameter that affects the heat transfer and it could be analyzed by awareness of the temperature distribution of the working fluid near the flow channel wall. The heat transfer coefficient is written as:

$$h = \frac{-k_f \left(\frac{\partial T}{\partial y} \right)_{y=0}}{T_w - T_b} \quad (15)$$

where T_w is the flow channel wall temperature, T_b is the bulk temperature of the fluid and y is the axis perpendicular to the flow direction. By applying a scale analysis in the thermal boundary layer of thickness δ_T , the heat transfer coefficient can be given as follows [36,42]:

$$h \sim \frac{k_f \left(\frac{\Delta T}{\delta_T} \right)}{\Delta T} \sim \frac{k_f}{\delta_T} \quad (16)$$

Hence reduction of the thermal boundary layer thickness in nanofluid flow could have a main role in thermal performance enhancement, and compensate the nanofluid low static thermal conductivity. Also from the microscopic point of view, the random movement of nanoparticles and re-arrangement because of non-uniform shear rate through the channel be attributed to heat transfer enhancement [43].

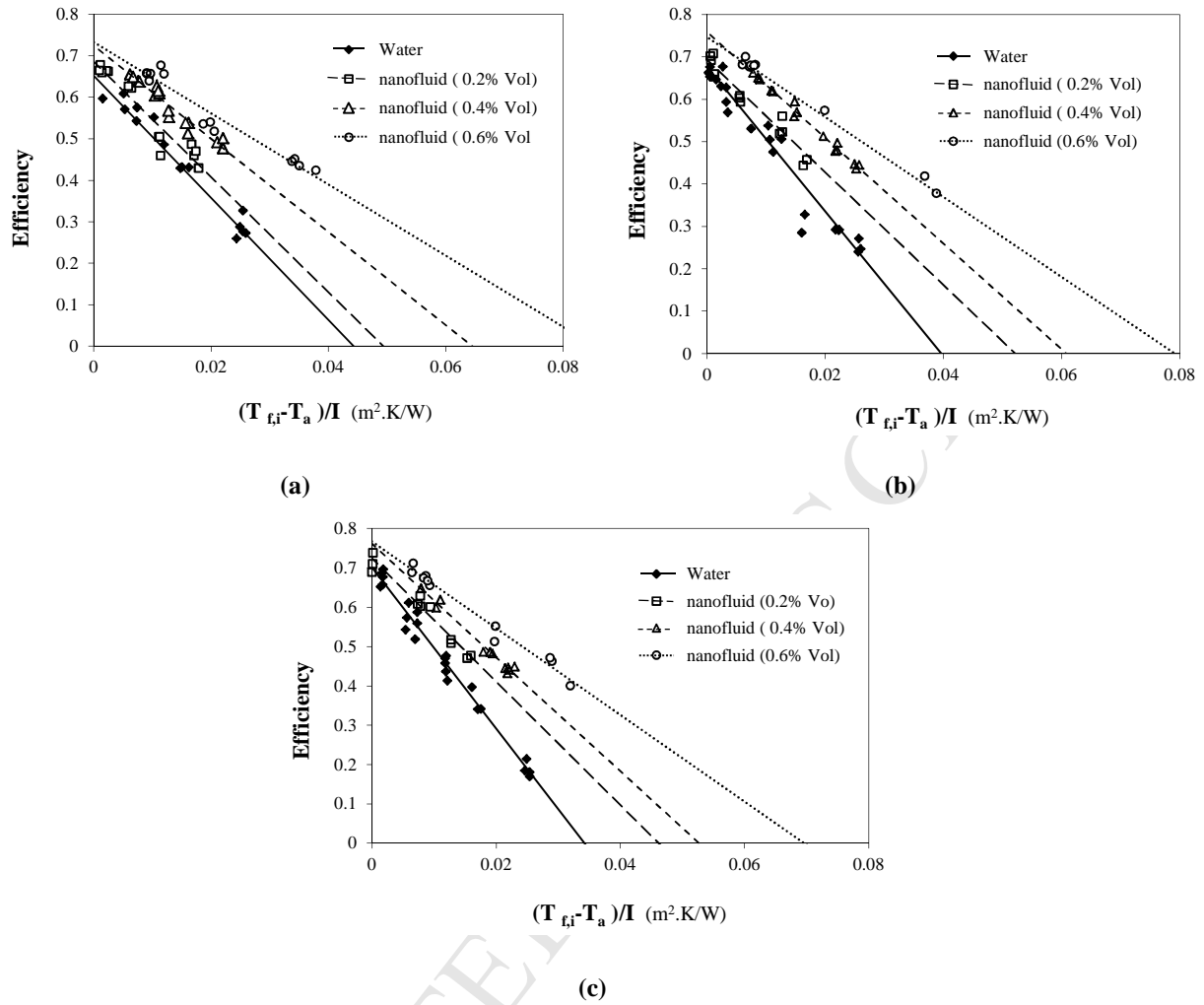


Fig. 7. Effect of nanofluid concentrations on the characteristic curves of the collector in different flow rate, (a) 0.5 lit/min , (b) 1 lit/min , (c) 1.5 lit/min

In Fig. 8, the effects of flow rate on the characteristic curves of the porous channel collector are separately shown in different nanofluid concentrations. Fig. 8a, shows the characteristic curves of deionized water. According to this figure, the pure water curves intersect each other in the reduced temperature parameter close to 0.009. So, these curves are divided into two regions with different dominant terms in Eq. (8). For reduced temperatures lower than about 0.009, $(T_{f,i} - T_a)/I < 0.009$, the efficiency has an increasing trend with an increase in the flow rate. Therefore, based on Eq. (8), $F_R(\tau\alpha)_e$ is more dominant term at lower reduced temperatures. An

305 opposite trend of the efficiency variations in greater reduced temperatures, points out that $F_R U_L$
 306 is more dominant parameter in reduced temperatures greater than 0.009. Also, the results of
 307 nanofluids flow, Fig. 8b-c, show the same behavior of the pure water characteristic curves. The
 308 intersection takes place at a mean reduced temperature greater than 0.015. The greater value of
 309 intersection point in nanofluids flow in comparison to the pure water is related to a reduction of
 310 the slope parameter of efficiency curves. Moreover, in each nanoparticle volume fraction the
 311 thermal efficiency variation with the flow rate is more considerable in greater values of the
 312 reduced temperature parameter.

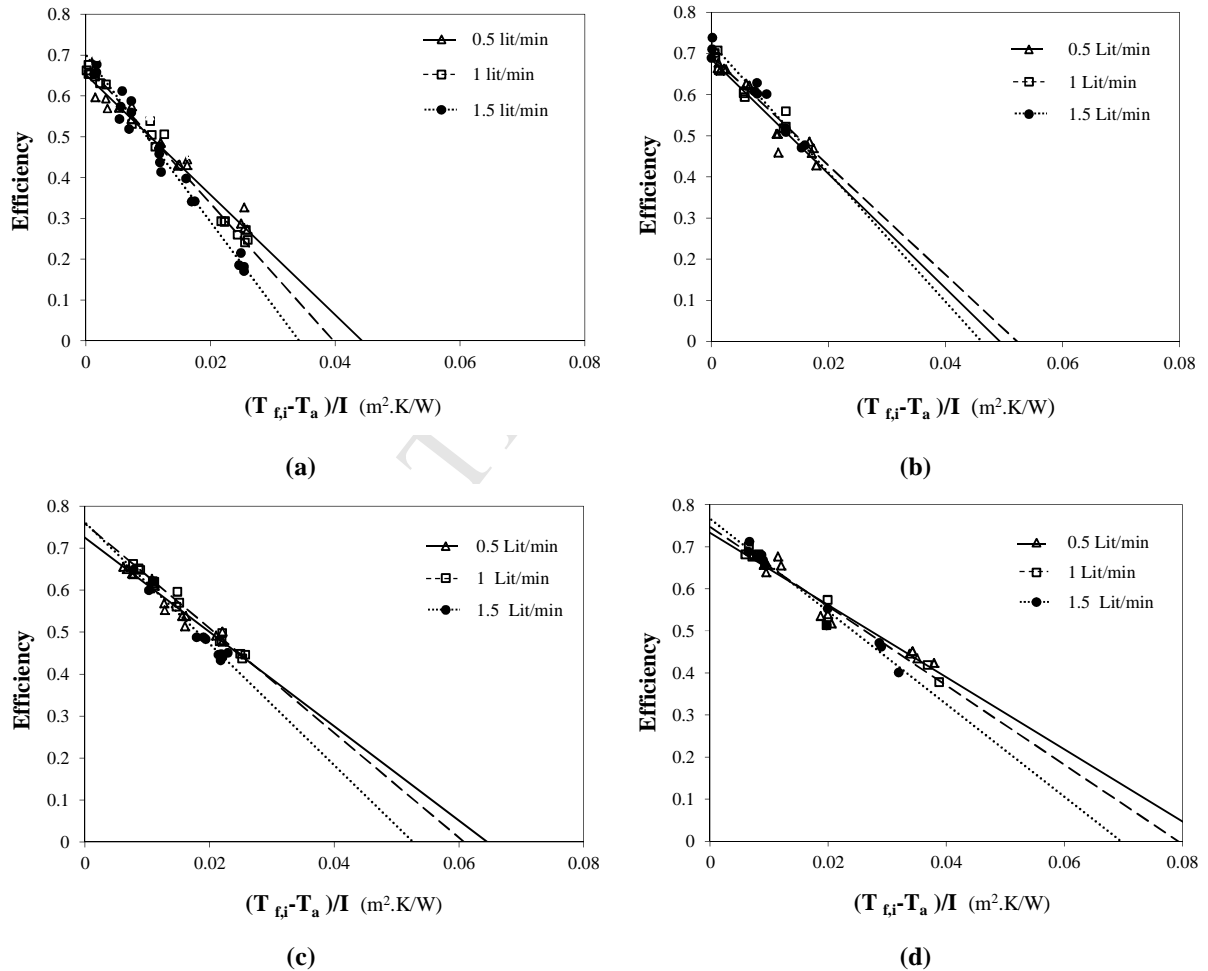


Fig. 8. Effect of flow rates on the characteristic curves of the collector in different nanofluid concentration, (a) 0%, (b) 0.2%, (c) 0.4%, (d) 0.6%

The extracted characteristics of efficiency curves for pure water and nanofluids are summarized in Table 4. It is seen that, nanofluid with higher concentration can cause higher absorbed energy parameter and also lower efficiency curve slope parameter.

Table 4. $F_R(\tau\alpha)_e$ and $F_R U_L$ of the collector for pure water and nanofluids

Nanofluids concentration	$F_R(\tau\alpha)_e$			$F_R U_L$		
	0.5 lit/min	1 lit/min	1.5 lit/min	0.5 lit/min	1 lit/min	1.5 lit/min
0% (deionized water)	0.652	0.677	0.7	14.74	17.05	20.47
0.2%	0.685	0.693	0.724	13.89	13.27	15.69
0.4%	0.724	0.758	0.762	11.23	12.46	14.45
0.6%	0.733	0.747	0.766	8.57	9.42	11.02

To have a better comparison of the efficiency characteristics, variations of the absorbed energy parameter and efficiency curve slope parameter are plotted in Figs. 9 and 10 versus the nanofluids concentration in different volume flow rates. As is evident from Fig. 9, the absorbed energy parameter rises with increasing the nanofluids concentration and flow rate. Also, the rate of increase in the absorbed energy parameter of the nanofluids reduces in volume fraction of 0.6%. This observation proposes using the smaller concentration (i. e. 0.4%), due to the more stability and lower cost of preparation of the suspension.

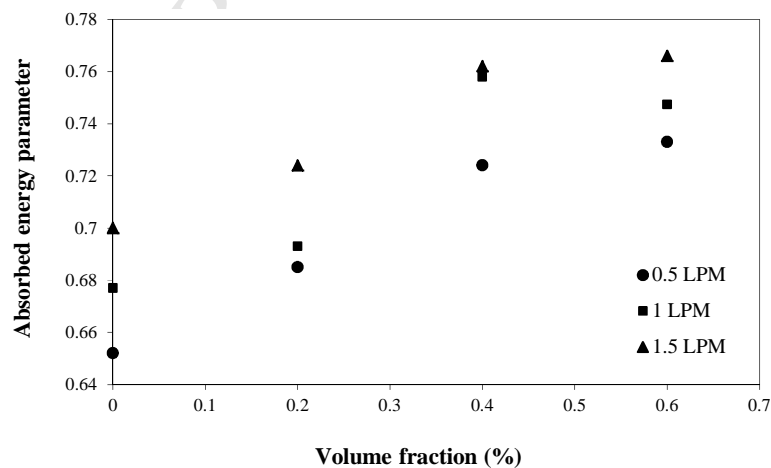


Fig. 9. Variations of the absorbed energy parameter versus nanofluid volume fraction in different flow rates

As observed in Fig. 10, using the nanofluid leads to a reduction in the efficiency curve slope parameter. This implies that the heat losses decrease in the nanofluid flow in comparison to the base fluid. Furthermore, the greater concentration has lower heat losses. Increasing of the efficiency curve slope parameter with growing the flow rate in each concentration is another prominent feature of this figure. This phenomenon can be elucidated by perusing the governing energy equation in porous media.

$$\frac{1}{\alpha_{eff}} \left(u \frac{\partial T}{\partial x} + v \frac{\partial T}{\partial y} \right) = \left(\frac{\partial^2 T}{\partial x^2} + \frac{\partial^2 T}{\partial y^2} \right) \quad (17)$$

in which α_{eff} is aggregate thermal diffusivity of the fluid-saturated porous media, u and v are flow velocity components in x and y directions, respectively. By neglecting the velocity in y direction, the equilibrium between three major possible effects in the energy equation consists of one term of longitudinal convection (enthalpy flow) and two terms of heat conduction in the porous media channel width and longitude. Based on a scale analysis of the main parameters of the energy equation, one can obtain:

$$\underbrace{\frac{hD}{K_{eff}}}_{\text{convection}}, \quad \underbrace{1}_{\text{width}}, \quad \underbrace{\left(\frac{hD}{K_{eff}} \right)^2}_{\text{longitudinal}} Pe^{-2} \quad (18)$$

where D is channel width, and K_{eff} is aggregate thermal conductivity of the fluid-saturated porous media. It is concluded that in the limit of large values of Peclet number (i. e. $Pe = Re.pr$) the conduction in the porous media channel length is insignificant in comparison to the conduction in width [42]. The larger values of the Peclet number are related to the larger values of flow rate or fluid velocity. Moreover, by increasing the working fluid velocity in the porous media, the timescale of solid thermal conduction for transferring the occupied thermal inertia to

the working fluid reduces. The reliability of this statement increases as the thermal conductivity ratio of the solid phase to the fluid phase is much larger than unity [44]. In conclusion, by increasing the working fluid velocity, contribution of the heat transfer caused by thermal conduction reduces in comparison to the thermal convection.

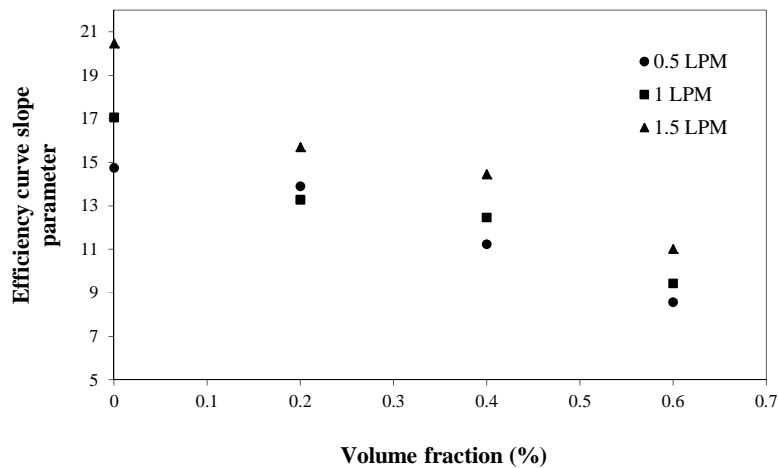


Fig. 10. Variations of the efficiency curve slope parameter versus nanofluid volume fraction in different flow rates

The Nusselt number as a non-dimensional parameter is applied to clarify the thermal performance of nanofluid flow through the collector channel. Here the Nusselt number is evaluated in the fluid inlet temperature close to the ambient temperature. The variations of the Nusselt number versus the flow rate in the porous channel collector are illustrated in Fig. 11. The obtained results are also compared against an empty channel collector with similar dimensions of Table 3. As shown, the Nusselt number improves by applying the metal foam in the flow channel. The Nusselt number is also enhanced by increasing the nanofluid volume concentration.

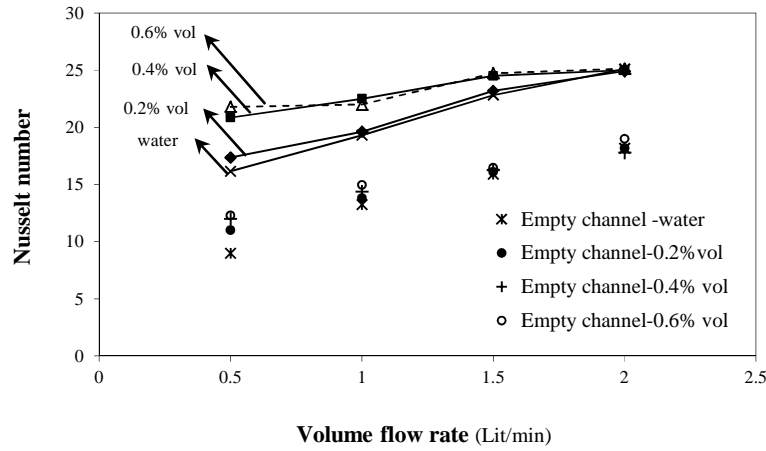


Fig. 11. Variations of the Nusselt number versus the volume flow rate (line for porous channel and without line for empty channel collector)

A relative enhancement of the Nusselt number in the porous channel collector is presented in Fig. 12. This parameter is defined as the ratio of the difference in the Nusselt number when the nanofluid is used instead of the pure water (i. e. $(Nu_{nf,p} - Nu_{w,p}) / Nu_{w,p}$). According to Fig. 12, the relative improvement of Nusselt number has a decreasing trend with raising the flow rate. In each nanofluid volume concentration, the relative improvement of the Nusselt number is also more remarkable in lower flow rate.

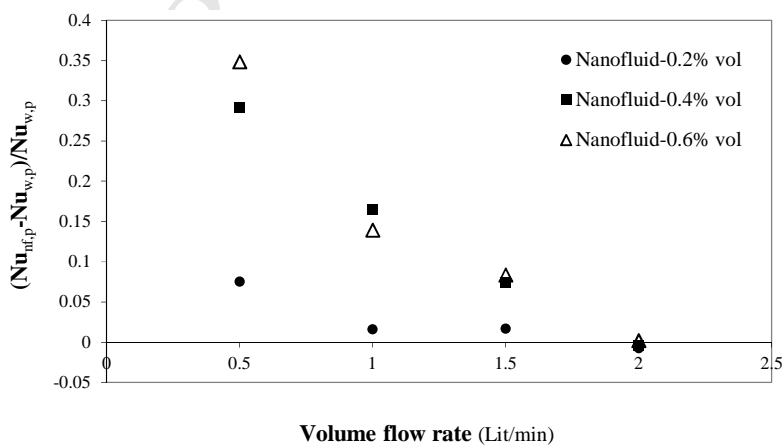


Fig. 12. Relative enhancement of the Nusselt number in the porous channel collector

Fig. 13 exhibits the values of pressure drop in the porous channel collector. A comparison is also performed with the measured data in the empty channel collector. A significant increase in the pressure drop is observed by using the porous media, especially at high volume flow rates, because the solid phase obstacle becomes more considerable in comparison to the surface friction [42]. Moreover, in both channels, the pressure drop has an increasing trend with raising the nanofluid concentration.

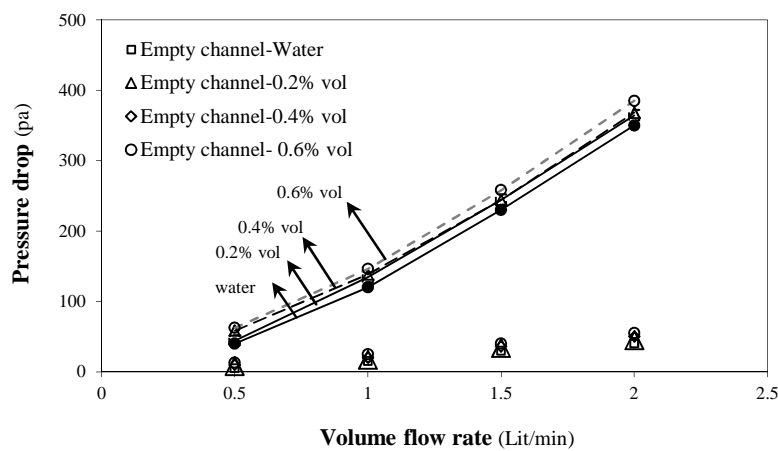


Fig. 13. Variations of the pressure drop versus the volume flow rate (line for porous channel and without line for empty channel collector)

Fig. 14 displays a Performance Evaluation Criterion (PEC) of the channel filled with metal foam, which both the heat transfer and pressure drop have been considered simultaneously [38,45]. The variations of nanofluid PEC, $PEC_{nf} = (Nu_{nf} / Nu_w) / (\Delta P_{nf} / \Delta P_w)^{1/3}$, versus flow rate have been evaluated in Fig. 14a. Although using the nanofluid instead of the base fluid can improve the heat transfer, an undesirable increase of the pressure drop is unavoidable. The results of this figure have a similar trend of the relative Nusselt number treatment in Fig. 12. The nanofluids PEC decreases with increasing the flow rate. Furthermore, the PEC of the nanofluids with 0.4% and 0.6% are close to each other. In Fig. 14b, another performance criterion definition is used to

376 evaluate the effect of porous media on the nanofluid flow. Based on the definition,
 377 $PEC_p = (Nu_{nf,p} / Nu_{nf,e}) / (\Delta P_{nf,p} / \Delta P_{nf,e})^{1/3}$, the nanofluid flow in the porous channel collector is
 378 compared with the nanofluid flow through the empty channel collector. As observed, PEC_p has
 379 a greater value in the higher nanoparticles volume fractions. It is also found that the variations of
 380 PEC_p versus the flow rate have a diminishing trend.

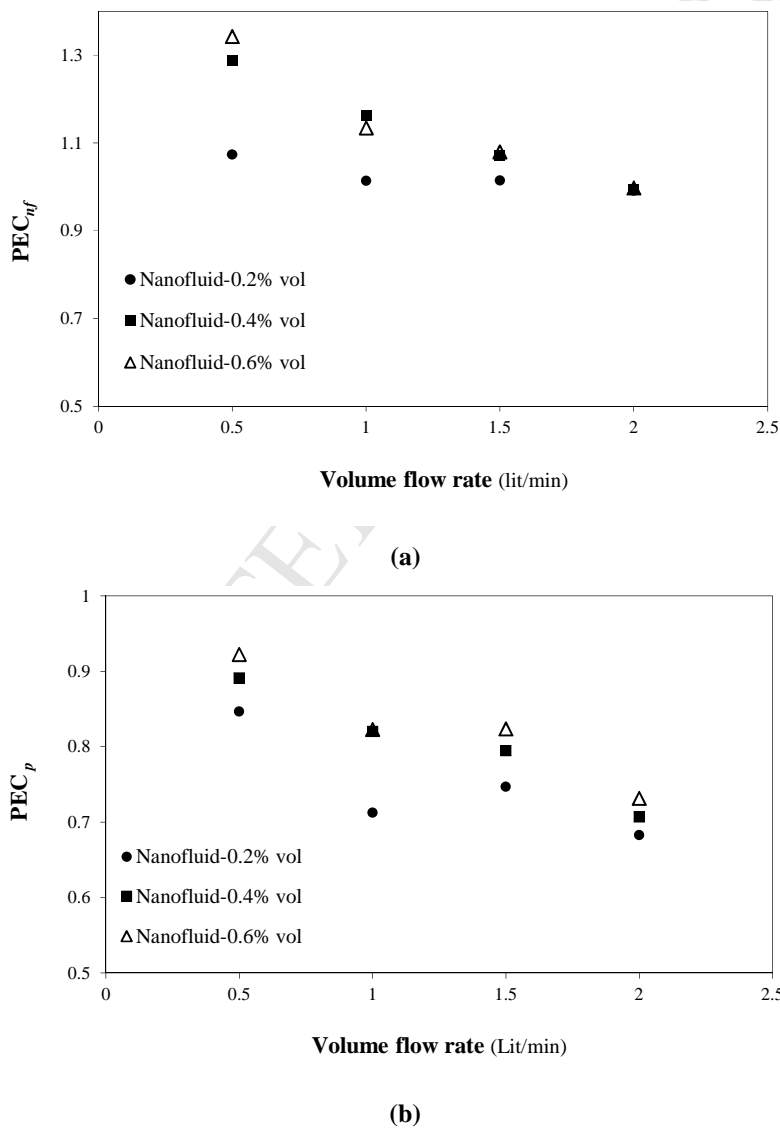


Fig. 14. Variations of the PEC versus the flow rate, (a) nanofluids PEC, (b) porous media PEC

3.3. The effect of nanoparticle size on the thermal performance

The SiO_2 nanoparticles sizes could have an important role in the thermal performance of the solar system [30,41]. Hence, the effect of nanoparticle size with the volume fraction of 0.6% has been investigated on the thermal efficiency of the porous channel collector. The results of this study for three different sizes of nanoparticles (i. e. 7 nm, 20-30 nm and 60-70 nm) and the flow rate of 1 lit/min are presented in Fig. 15 and Table 5. It is seen that the absorbed energy parameter, $F_R(\tau\alpha)_e$, and efficiency curve slope parameter, $F_R U_L$, for nanoparticle size of 60-70 nm is 0.697 and 10.12, respectively. The values of $F_R(\tau\alpha)_e$ and $F_R U_L$ improve in the characteristic curve of nanoparticle with average diameter of 20-30 nm. The curves of nanofluid with nanoparticles of 7nm and 20-30 nm intersected at the approximate reduced temperature parameter of 0.03. For reduced temperature parameter greater than the intersection point, $F_R U_L$ is more dominant and causes the greater efficiency of the nanofluid with smaller particle size. The nanoparticles sizes effects on the thermal efficiency can be explained by referring to the specific surface area of nanoparticles (Table 6), obtained from nitrogen adsorption analyzer. As expected, according to the analyze results, nanoparticles with smaller size has a greater specific area. It leads to a greater interfacial surface of the base fluid and nanoparticles, and increases the Brownian motion. So, it causes a relative improvement of the thermal conductivity and heat transfer process. As a conclusion of this section, the thermal performance of the porous channel collector with smaller nanoparticle size can be superior in comparison to the greater one.

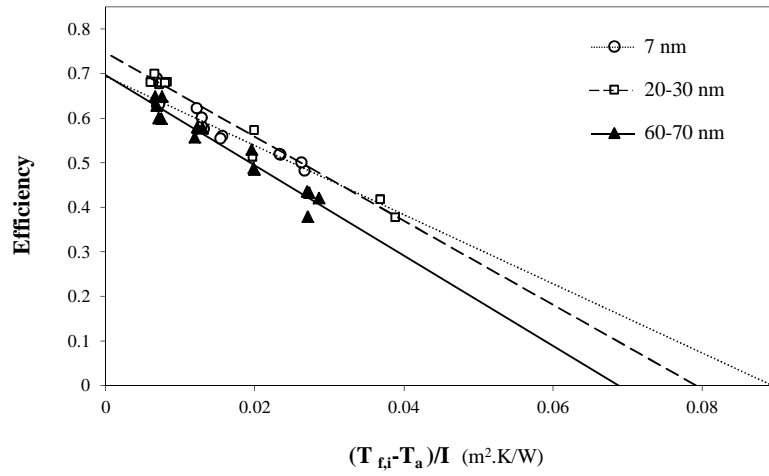


Fig. 15. Effect of nanoparticle size on the thermal efficiency of the porous channel collector (nanofluid with 0.6% vol. concentration)

Table 5. $F_R(\tau\alpha)_e$ and $F_R U_L$ for SiO₂ nanofluid with different nanoparticle sizes

Nanoparticle size (nm)	7	(20-30)	(60-70)
$F_R(\tau\alpha)_e$	0.694	0.747	0.697
$F_R U_L$	7.75	9.42	10.12

Table 6. Specific surface area of SiO₂ nanoparticle (results of nitrogen adsorption analyzer)

Nanoparticle size (nm)	7	(20-30)	(60-70)
BET surface area (m ² g ⁻¹)	237	232	225

4. Conclusions

In the present study, the thermal performance of a fully filled porous channel FPSC with the SiO₂/deionized water nanofluids was experimentally investigated. The experiments were performed base on ASHRAE standard at three volume flow rates and nanoparticle volume fractions of 0.2%, 0.4%, and 0.6%. Analysis of the results clarifies that despite their lower thermal conductivities, in comparison to the other conventional nanoparticles, SiO₂ nanoparticles have a considerable improvement on the thermal performance. Some highlights of the present investigation can be stated as follows:

- In the reduced temperature parameter close to zero, increasing the nanofluid volume concentration to 0.6% causes the thermal efficiency enhancement approximately between 6% and 8% in different flow rates.
 - By comparing the domain of the efficiency changes versus the nanofluid concentration and flow rate, it is found that the effect of the nanofluid concentration on the collector efficiency is greater than that of the flow rate.
 - The trend of the collector efficiency with the nanofluid flow rate is similar to the pure water. The characteristic curves intersect each other in a mean value of reduced temperature parameter greater than 0.015.
 - The greater values of flow rates are more effective at lower reduced temperature parameters. At higher reduced temperatures, a higher thermal efficiency is obtained at the smaller values of flow rates.
 - The variation of nanofluid performance, PEC_{nf} , with the flow rate has a decreasing trend. The nanofluids with 0.4% and 0.6% vol. have a performance close to each other.
 - Based on the definition for evaluating the effect of metal porous foam, PEC_p , in the channel with nanofluid flow, it is observed that with increasing the nanofluid concentration from 0.2% to 0.6%, PEC_p increases from 0.84 to 0.92 for the flow rate of 0.5 lit/min.
 - Finally, the efficiency curve slope parameter is directly proportional to the nanoparticle size.
- As a result, this experimental study would present a better insight into the simultaneous use of nanofluids and porous media in FPSC. The thermal efficiency improvement of FPSC can diminish its dimensions and get a higher fluid outlet temperature for more utilization in domestic and industrial hot water.

Acknowledgment

The first, second, third and fourth authors thank Iran National Science Foundation: INSF for the support. The fifth author acknowledges the support provided by the "Research Chair Grant" National Science and Technology Development Agency (NSTDA), the Thailand Research Fund (TRF), the National Research University Project (NRU) and King Mongkut's University of Technology Thonburi through the "KMUTT 55th Anniversary Commemorative Fund".

Nomenclature

A_c	Collector surface (m ²)	x, y	Cartesian coordinates (m)
A_p	Heat transfer surface (m ²)	Greek letters	
C_p	Specific heat at constant pressure (J/kg.K)	α	Thermal diffusivity (m ² /s)
D_h	Hydraulic diameter (m)	δ	Uncertainty
d_{np}	Nanoparticle size (m)	δ_T	Thermal boundary layer thickness (m)
F_R	Collector heat removal factor	η	Collector performance efficiency
F'	Collector efficiency factor	μ	Viscosity (kg/m.s)
h	Convection heat transfer coefficient (W/m ² .K)	ρ	Density (kg/m ³)
I	Incident solar irradiation (W/m ²)	$(\tau\alpha)_e$	Effective transmission- absorption coefficient
K	Thermal conductivity (W/m.K)	ϕ	Volume fraction
k_B	Boltzmann constant (J/K)	Subscripts	
\dot{m}	Mass flow rate (kg/s)	a	Ambient
Nu	Nusselt number	e	Empty channel
P	Pressure (Pa)	eff	Effective property in porous media
\dot{Q}	Volume flow rate (m ³ /s)	f	Base fluid
\dot{Q}_u	Useful gain of energy (W)	i	Inlet
T	Temperature (K)	nf	Nanofluid
u, v	Flow velocity in x and y directions, respectively (m/s)	o	Outlet
U_L	Loss coefficient (W/m ² .K)	p	Porous channel
		np	Nanoparticle
		w	Wall
		w	Deionized water

References

- [1] D.G. Gunjo, P. Mahanta, P.S. Robi, CFD and experimental investigation of flat plate solar water heating system under steady state condition, *Renew. Energy* 106 (2017) 24–36.
- [2] E. Bellos, C. Tzivanidis, Parametric analysis and optimization of an Organic Rankine Cycle with nanofluid based solar parabolic trough collectors, *Renew. Energy* (2017). doi:10.1016/j.renene.2017.06.055.
- [3] U. Diego-ayala, J.G. Carrillo, Evaluation of temperature and efficiency in relation to mass flow on a solar flat plate collector in Mexico, *Renew. Energy* 96 (2016) 756–764.
- [4] S.A. Kalogirou, S. Karellas, V. Badescu, K. Braimakis, Exergy analysis on solar thermal systems: A better understanding of their sustainability, *Renew. Energy* 85 (2016) 1328–1333.
- [5] T. Yousefi, E. Shojaeizadeh, F. Veysi, S. Zinadini, An experimental investigation on the effect of pH variation of MWCNT-H₂O nanofluid on the efficiency of a flat-plate solar collector, *Sol. Energy* 86 (2) (2012) 771–779.
- [6] Y. Li, J. Fernandez-seara, K. Du, A.A. Pardinas, L.L. Latas, W. Jiang, Experimental investigation on heat transfer and pressure drop of ZnO/Ethylene Glycol-Water nanofluids in transition flow, *Appl. Therm. Eng.* 93 (2016) 537–548.
- [7] E. Shojaeizadeh, F. Veysi, T. Yousefi, F. Davodi, An experimental investigation on the efficiency of a Flat-plate solar collector with binary working fluid: A case study of propylene glycol (PG)-water, *Exp. Therm. Fluid Sci.* 53 (2014) 218–226.
- [8] ANSI/ASHRAE Standard 93, Methods of Testing to Determine the Thermal Performance of Solar Collectors, 2003. Atlanta, GA, USA.
- [9] T. Yousefi, F. Veysi, E. Shojaeizadeh, S. Zinadini, An experimental investigation on the effect of Al₂O₃-H₂O nanofluid on the efficiency of flat-plate solar collectors, *Renew. Energy* 39 (2012) 293–298.
- [10] M.T. Jamal-abad, A. Zamzamian, E. Imani, M. Mansouri, Experimental Study of the Performance of a Flat-Plate Collector Using Cu-Water Nanofluid, *J. Thermophys. Heat Transf.* 27 (2013) 756–760.
- [11] A. Zamzamian, M. Keyanpourrad, M. Kianineyestani, M.T. Jamal-abad, An experimental study on the effect of Cu-synthesized/EG nano fluid on the efficiency of flat-plate solar collectors, *Renew. Energy* 71 (2014) 658–664.
- [12] S. Salavati, A. Kianifar, H. Niazmand, O. Mahian, S. Wongwises, Experimental investigation on the thermal efficiency and performance characteristics of a flat plate solar collector using SiO₂/EG–water nanofluids, *Int. Commun. Heat Mass Transf.* 65 (2015) 71–75.
- [13] D.A. Vincely, E. Natarajan, Experimental investigation of the solar FPC performance using graphene oxide nanofluid under forced circulation, *Energy Convers. Manag.* 117 (2016) 1–11.
- [14] M.T. Jamal-abad, S. Saedodin, M. Aminy, Heat transfer in concentrated solar air-heaters filled with a porous medium with radiation effects: A perturbation solution, *Renew. Energy* 91 (2016) 147–154.
- [15] S. Rashidi, J.A. Esfahani, A. Rashidi, A review on the applications of porous materials in solar energy systems, *Renew. Sustain. Energy Rev.* 73 (2017) 1198–1210.

- 479 [16] M.A. Al-Nimr, M.K. Alkam, A Modified Tubeless Solar Collector Partially Filled with porous
480 Substrate, *Renew. Energy* 13 (1998) 165–173.
- 481 [17] M.K. Alkam, M.A. Al-Nimr, Solar Collectors with Tubes Partially Filled with Porous Substrates,
482 *J. Sol. Energy Eng. Trans. ASME*. 121 (1999) 20–24.
- 483 [18] C. Chen, P. Huang, Numerical study of heat transfer enhancement for a novel flat-plate solar water
484 collector using metal-foam blocks, *Int. J. Heat Mass Transf.* 55 (2012) 6734–6756.
- 485 [19] P. Huang, C. Chen, H. Hwang, Thermal enhancement in a flat-plate solar water collector by flow
486 pulsation and metal-foam blocks, *Int. J. Heat Mass Transf.* 61 (2013) 696–720.
- 487 [20] S. Hirasawa, R. Tsubota, T. Kawanami, K. Shirai, Reduction of heat loss from solar thermal
488 collector by diminishing natural convection with high-porosity porous medium, *Sol. Energy* 97
489 (2013) 305–313.
- 490 [21] H. Xu, L. Gong, S. Huang, M. Xu, Non-equilibrium heat transfer in metal-foam solar collector
491 with no-slip boundary condition, *Int. J. Heat Mass Transf.* 76 (2014) 357–365.
- 492 [22] S. Rashidi, M. Bovand, J.A. Esfahani, Heat transfer enhancement and pressure drop penalty in
493 porous solar heat exchangers: A sensitivity analysis, *Energy Convers. Manag.* 103 (2015) 726–
494 738.
- 495 [23] M. Dehghan, Y. Rahmani, D. Domiri, S. Saedodin, Convection-radiation heat transfer in solar heat
496 exchangers filled with a porous medium: Homotopy perturbation method versus numerical
497 analysis, *Renew. Energy* 74 (2015) 448–455.
- 498 [24] M. Bovand, S. Rashidi, J.A. Esfahani, Heat transfer enhancement and pressure drop penalty in
499 porous solar heaters: Numerical simulations, *Sol. Energy* 123 (2016) 145–159.
- 500 [25] S. Rashidi, M. Bovand, J.A. Esfahani, Sensitivity Analysis for Entropy Generation in Porous Solar
501 Heat Exchangers by RSM, *J. Thermophys. Heat Transf.* 31 (2) (2017) 390–402.
- 502 [26] O.K. Ahmed, Z.A. Mohammed, Influence of porous media on the performance of hybrid
503 PV/Thermal collector, *Renew. Energy* 112 (2017) 378–387.
- 504 [27] M.A. Adriana, Hybrid nanofluids based on Al_2O_3 , TiO_2 and SiO_2 : Numerical evaluation of
505 different approaches, *Int. J. Heat Mass Transf.* 104 (2017) 852–860.
- 506 [28] K. Khanafer, K. Vafai, A critical synthesis of thermophysical characteristics of nanofluids, *Int. J.*
507 *Heat Mass Transf.* 54 (2011) 4410–4428.
- 508 [29] M. Hajipour, A.M. Dehkordi, Mixed-convection flow of Al_2O_3 - H_2O nanofluid in a channel
509 partially filled with porous metal foam: Experimental and numerical study, *Exp. Therm. Fluid Sci.*
510 53 (2014) 49–56.
- 511 [30] O. Mahian, A. Kianifar, A.Z. Sahin, S. Wongwises, Heat Transfer, Pressure drop and Entropy
512 generation in a solar collector using SiO_2 /water nanofluids: Effects of nanoparticle size and pH,
513 *ASME, J. Heat Transf.* 137 (6) (2015).
- 514 [31] H.C. Brinkman, The Viscosity of Concentrated Suspensions and Solutions, *J. Chem. Phys.* 20 (4)
515 (1952) 571.
- 516 [32] M. Tajik Jamal-abad, S. Saedodin, M. Aminy, Experimental investigation on a solar parabolic
517 trough collector for absorber tube filled with porous media, *Renew. Energy* 107 (2017) 156–163.
- 518 [33] D. Rojas, J. Beermann, S.A. Klein, D.T. Reindl, Thermal performance testing of flat-plate
519 collectors, *Sol. Energy* 82 (8) (2008) 746–757.

- [34] J. A. Duffie, W.A. Beckman, *Solar Engineering of Thermal Processes*, fourth ed., John Wiley & Sons, Inc., 2013.
- [35] S.A. Kalogirou, *Solar Energy Engineering: Processes and Systems*, first ed., Elsevier, Oxford, 2009.
- [36] A. Bejan, *Convection Heat Transfer*, third ed., John Wiley & Sons, Inc., Canada, 2004.
- [37] M. Faizal, R. Saidur, S. Mekhilef, A. Hepbasli, I.M. Mahbubul, Energy, economic, and environmental analysis of a flat-plate solar collector operated with SiO₂ nanofluid, *Clean Tech. Env. Policy* 17 (6) (2014) 1457–1473.
- [38] M. Nazari, M. Ashouri, M.H. Kayhani, A. Tamayol, Experimental study of convective heat transfer of a nanofluid through a pipe filled with metal foam, *Int. J. Therm. Sci.* 88 (2015) 33–39.
- [39] R.J. Moffat, Using Uncertainty Analysis in the Planning of an Experiment, *J. Fluids Eng.* 107 (1985) 173–178.
- [40] L. Jiang, L. Gao, J. Sun, Production of aqueous colloidal dispersions of carbon nanotubes, *J. Colloid Interface Sci.* 260 (2003) 89–94.
- [41] O. Mahian, A. Kianifar, S.Z. Heris, D. Wen, A.Z. Sahin, S. Wongwises, Nanofluids effects on the evaporation rate in a solar still equipped with a heat exchanger, *Nano Energy* 36 (2017) 134–155.
- [42] D.A. Nield, A. Bejan, *Convection in Porous Media*, third ed., Springer, NY, 2006.
- [43] M.A. Alim, Z. Abdin, R. Saidur, A. Hepbasli, M.A. Khairul, N.A. Rahim, Analyses of Entropy Generation and Pressure Drop for a Conventional Flat Plate Solar Collector Using Different Types of Metal Oxide Nanofluids, *Energy Build.* 66 (2013) 289–296.
- [44] K. Vafai, *handbook of porous media*, second ed., CRC Press, Taylor & Francis Group, 2005.
- [45] M.E. Nimvari, M. Maerefat, M.K. El-hossaini, Numerical simulation of turbulent flow and heat transfer in a channel partially filled with a porous media, *Int. J. Therm. Sci.* 60 (2012) 131–141.